Article

Protein Film Voltammetry of Copper-Containing Nitrite Reductase Reveals Reversible Inactivation

Hein J. Wijma, Lars J. C. Jeuken, Martin Ph. Verbeet, Fraser A. Armstrong, and Gerard W. Canters

J. Am. Chem. Soc., **2007**, 129 (27), 8557-8565• DOI: 10.1021/ja071274q • Publication Date (Web): 19 June 2007

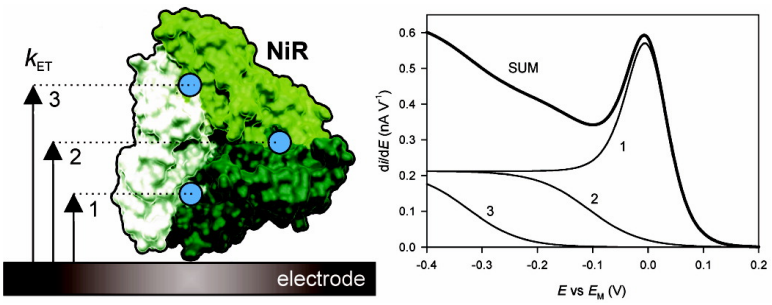

More About This Article

Additional resources and features associated with this article are available within the HTML version:

- Supporting Information
- Links to the 5 articles that cite this article, as of the time of this article download
- Access to high resolution figures
- Links to articles and content related to this article
- Copyright permission to reproduce figures and/or text from this article

View the Full Text HTML

J|A|C|S
ARTICLES
Published on Web 06/19/2007

Protein Film Voltammetry of Copper-Containing Nitrite Reductase Reveals Reversible Inactivation

Hein J. Wijma,[†,‡] Lars J. C. Jeuken,[§] Martin Ph. Verbeet,[†] Fraser A. Armstrong,[#] and Gerard W. Canters*[,†]

Contribution from the Leiden Institute of Chemistry, Leiden University, P.O. Box 9502, 2300 RA Leiden, The Netherlands, School of Physics and Astronomy, University of Leeds, Leeds LS2 9JT, U.K., and Inorganic Chemistry Laboratory, Oxford University, South Parks Road, Oxford OX1 3QR, U.K.

Received February 22, 2007; E-mail: canters@chem.leidenuniv.nl

Abstract: The Cu-containing nitrite reductase from *Alcaligenes faecalis* S-6 catalyzes the one-electron reduction of nitrite to nitric oxide (NO). Electrons enter the enzyme at the so-called type-1 Cu site and are then transferred internally to the catalytic type-2 Cu site. Protein film voltammetry experiments were carried out to obtain detailed information about the catalytic cycle. The homotrimeric structure of the enzyme is reflected in a distribution of the heterogeneous electron-transfer rates around three main values. Otherwise, the properties and the mode of operation of the enzyme when it is adsorbed as a film on a pyrolytic graphite electrode are essentially unchanged compared to those of the free enzyme in solution. It was established that the reduced type-2 site exists in either an active or an inactive conformation with an interconversion rate of $\sim$0.1 s^{-1}. The random sequential mechanism comprises two routes, one in which the type-2 site is reduced first and subsequently binds nitrite, which is then converted into NO, and another in which the oxidized type-2 site binds nitrite and then accepts an electron to produce NO. At high nitrite concentration, the second route prevails and internal electron transfer is rate-limiting. The midpoint potentials of both sites could be established under catalytic conditions. Binding of nitrite to the type-2 site does not affect the midpoint potential of the type-1 site, thereby excluding cooperativity between the two sites.

Introduction

Copper-containing nitrite reductase (NiR) is an important enzyme in denitrifying microorganisms, including many bacteria, archaea, and fungi,[1−3] in which it catalyzes the one-electron reduction of nitrite to nitric oxide:

$$NO_2^- + 2H^+ + e^- \rightleftarrows NO + H_2O \qquad (1)$$

This reaction is an important step in the denitrification pathway. The enzyme catalyzes bidirectionally, and the maximum rates of the forward and reverse reactions are approximately the same at pH 7.5.[4] NiR is known to enhance resistance to human sera in *Neisseria gonorrhoeae*,[5] and it allows *Neisseria meningitidis* to respire on nitrite under the microaerobic conditions encountered during host colonization and disease.[6] There is also an interest[7−9] in applying NiR in amperometric biosensors to monitor nitrite in body fluids, natural streams, and wastewaters.

NiR is a homotrimer[10] in which each subunit contains a type-1 Cu electron-transfer (ET) site and a type-2 Cu catalytic site.[11,12] The type-1 site is near the surface and accepts an electron from a physiological electron donor, like pseudo-azurin,[13−15] before transferring it to the buried catalytic type-2 site. The type-2 Cu is coordinated by the N_ϵ atoms of three histidine residues, with the fourth coordination position being available for binding nitrite.[16] Two other conserved residues in the active site, an

[†] Leiden University.
[§] University of Leeds.
[#] Oxford University.
[‡] Current address: Department of Biochemistry, Duke University Medical Center, Durham, NC 27710.

(1) Zumft, W. G. *Microbiol. Mol. Biol. Rev.* **1997**, *61*, 533−616.
(2) Ichiki, H.; Tanaka, Y.; Mochizuki, K.; Yoshimatsu, K.; Sakurai, T.; Fujiwara, T. *J. Bacteriol.* **2001**, *183*, 4149−4156.
(3) Adman, E. T.; Murphy, M. E. P. In *Handbook of Metalloproteins*; Messerschmidt, A., Huber, R., Poulos, T., Wieghardt, K., Eds.; John Wiley & Sons, Ltd.: Chicester, 2001; Vol. 2, pp 1381−1390.
(4) Wijma, H. J.; Canters, G. W.; de Vries, S.; Verbeet, M. P. *Biochemistry* **2004**, *43*, 10467−10474.
(5) Cardinale, J. A.; Clark, V. L. *Infect. Immun.* **2000**, *68*, 4368−4369.
(6) Rock, J. D.; Moir, J. W. *Biochem. Soc. Trans.* **2005**, *33*, 134−136.
(7) Sasaki, S.; Karube, I.; Hirota, N.; Arikawa, Y.; Nishiyama, M.; Kukimoto, M.; Horinouchi, S.; Beppu, T. *Biosens. Bioelectron.* **1998**, *13*, 1−5.
(8) Wu, Q.; Storrier, G. D.; Pariente, F.; Wang, Y.; Shapleigh, J. P.; Abruña, H. D. *Anal. Chem.* **1997**, *69*, 4856−4863.
(9) Astier, Y.; Canters, G. W.; Davis, J. J.; Hill, H. A. O.; Verbeet, M. P.; Wijma, H. J. *ChemPhysChem* **2005**, *6*, 1114−1120.
(10) Godden, J. W.; Turley, S.; Teller, D. C.; Adman, E. T.; Liu, M. Y.; Payne, W. J.; LeGall, J. *Science* **1991**, *253*, 438−442.
(11) Kukimoto, M.; Nishiyama, M.; Murphy, M. E.; Turley, S.; Adman, E. T.; Horinouchi, S.; Beppu, T. *Biochemistry* **1994**, *33*, 5246−5252.
(12) Libby, E.; Averill, B. A. *Biochem. Biophys. Res. Commun.* **1992**, *187*, 1529−1535.
(13) Kukimoto, M.; Nishiyama, M.; Ohnuki, T.; Turley, S.; Adman, E. T.; Horinouchi, S.; Beppu, T. *Protein Eng.* **1995**, *8*, 153−158.
(14) Kukimoto, M.; Nishiyama, M.; Tanokura, M.; Adman, E. T.; Horinouchi, S. *J. Biol. Chem.* **1996**, *271*, 13680−13683.
(15) Kakutani, T.; Watanabe, H.; Arima, K.; Beppu, T. *J. Biochem. (Tokyo)* **1981**, *89*, 463−472.
(16) Adman, E. T.; Godden, J. W.; Turley, S. *J. Biol. Chem.* **1995**, *270*, 27458−27474.

Scheme 1. Proposed Catalytic Cycle of NiR[a]

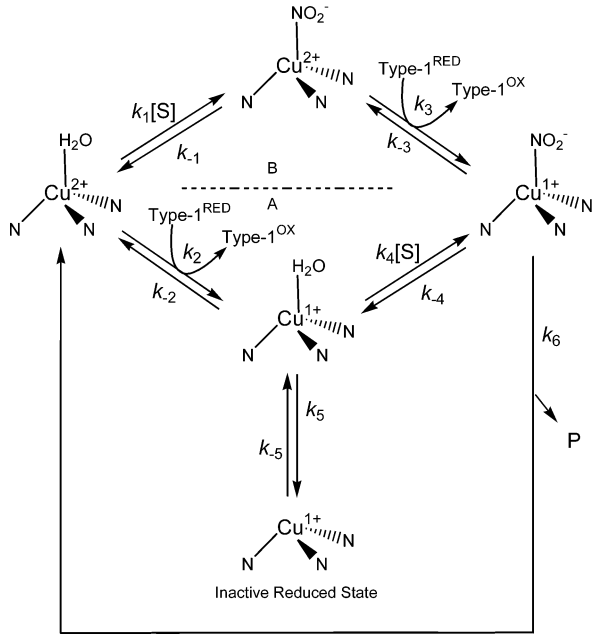

[a] Depicted is the type-2 Cu site, where the catalytic conversion of nitrite to NO takes place. At the left, the site is in the oxidized form. It may accept a nitrite ion and then an electron from the type-1 site (upper route, labeled B) or first an electron and then the nitrite (lower route, labeled A). The reduced species in the lower route may (reversibly) convert to an inactive, three-coordinate species (step 5). In step 6, the nitrite is converted to NO, and the reaction cycle is closed. The nitrite is depicted as deprotonated, but it may also be protonated in the catalytic cycle. The type-2 Cu atom is depicted with the N_ϵ atoms of the ligating histidines. The scheme applies at low pH. At high pH, the water molecules coordinating to the type-2 Cu are replaced by hydroxyl groups.

aspartate and a histidine, are needed for efficient catalysis.[17−20] As shown previously, during the catalytic cycle, nitrite binding and type-2 site reduction may occur in random order; i.e., the type-2 Cu can be reduced before (A) or after (B) binding of NO_2^- (Scheme 1).[21] The steady-state rate of reduction is given by[21]

$$k_t = k_{cat}^{A}[NO_2^-]\left(\frac{1 + (k_{cat}^{B}/k_{cat}^{A})([NO_2^-]/K_M^{B})}{K_M^{A} + [NO_2^-] + ([NO_2^-]^2/K_M^{B})}\right) \quad (2)$$

in which k_t is the turnover rate of NiR, K_M^A and K_M^B are the Michaelis constants for the A and B routes in Scheme 1, respectively, and k_{cat}^A and k_{cat}^B are the rate constants for the A and B routes.[21] Below pH 6.5, $k_{cat}^B < k_{cat}^A$, and above pH 6.5 the reverse holds.

Elsewhere[21] we presented evidence for the existence of the two routes depicted in Scheme 1. However, the occurrence of a fifth step, representing the equilibrium between active and inactive forms of the enzyme,[22] could not be established definitely. The present work focuses on the behavior of the enzyme when immobilized on a graphite electrode and, in particular, on the transition of the active into the inactive form and *vice versa*. Protein film voltammetry (PFV),[23−25] in which a film of enzyme molecules is immobilized on an electrode, is an attractive technique for studying redox-active enzymes because it probes the potential dependence of catalytic activity (the rate is measured directly as current) and reveals aspects that are normally not resolved with traditional methods. This study focuses on the catalytic activity of the immobilized redox enzyme as a function of electrode potential, substrate concentration, and time. The homotrimeric structure of the enzyme is reflected in the distribution of the ET rates. Quantitative information is provided on a slow isomerization between an inactive reduced state (IRS) and a "normal" reduced type-2 site. At saturating nitrite concentrations, we find that the type-1 → type-2 electron transfer is the rate-limiting step, and we establish that the midpoint potential of the type-1 site is not altered by the binding of nitrite to the nearby type-2 site.

Materials and Methods

General. Wild-type NiR from *Alcaligenes faecalis* S-6 was prepared as described[4] with omission of the gel filtration step, which did not improve the response on the electrode. All experiments were carried out with a rotating disk pyrolytic graphite edge (PGE) working electrode described previously.[21] For NiR immobilization, the PGE electrode was polished thoroughly on a polishing cloth (Buehler) covered with 6 μm diamond, sonicated in H_2O, washed with buffer, exposed to NiR (>100 μM) for 30 s, rinsed with H_2O, and inserted in the buffer. After the cell was sealed, oxygen was removed by purging the solution with water-saturated argon for several minutes. Subsequently, the electrode was cycled between 560 and −140 mV to verify that oxygen was absent. Anaerobic conditions were maintained during the experiment by flushing the headspace with argon. Potentials are quoted versus the normal hydrogen electrode (NHE). Voltammograms were measured using an Autolab electrochemical analyzer (EcoChemie, Utrecht, The Netherlands). The typical rotation rate of the working electrode was 2000 rpm, and it was ascertained that faster rotation did not increase the current, regardless of nitrite concentration. The kinetic constants K_M^A, K_M^B, and k_{cat}^B/k_{cat}^A were determined as described in ref 21. Potentiometric titrations were carried out as described in ref 26. Nitric oxide gas (British Oxygen Co. (BOC), 0.5% NO in 99.5% N_2) was scrubbed with 1 M KOH and 0.1 M potassium phosphate, pH 7, prior to application. Bubbling with this gas-mixture gives a 16 μM nitric oxide solution at 1 °C.[27] Unless mentioned otherwise, all experiments were carried out with the sample cell maintained at 1 ± 1 °C. This temperature was chosen to stabilize the protein film formed on the electrode surface.[21]

Pre-Steady-State Kinetics. The enzyme kinetics were studied by starting with the fully reduced or oxidized enzyme, applying a change in the electrode potential, and watching the kinetics reach a steady state. Referring to the catalytic cycle shown in Scheme 1, if k_5 and k_{-5} are much slower than the other steps, then k_t (the catalytic turnover rate) will change exponentially with time to reach its steady-state value. When the assay is initiated with oxidized enzyme, k_t will decrease with time (the assay starts with 100% active enzyme and part of it ends up in the IRS), whereas when the assay is initiated with reduced enzyme (where there is an equilibrium between active reduced enzyme and

(17) Murphy, M. E.; Turley, S.; Adman, E. T. *J. Biol. Chem.* **1997**, *272*, 28455−28460.
(18) Boulanger, M. J.; Murphy, M. E. *Biochemistry* **2001**, *40*, 9132−9141.
(19) Boulanger, M. J.; Kukimoto, M.; Nishiyama, M.; Horinouchi, S.; Murphy, M. E. *J. Biol. Chem.* **2000**, *275*, 23957−23964.
(20) Kataoka, K.; Furusawa, H.; Takagi, K.; Yamaguchi, K.; Suzuki, S. *J. Biochem.* (*Tokyo*) **2000**, *127*, 345−350.
(21) Wijma, H. J.; Jeuken, L. J.; Verbeet, M. P.; Armstrong, F. A.; Canters, G. W. *J. Biol. Chem.* **2006**, *281*, 16340−16346.
(22) Strange, R. W.; Murphy, L. M.; Dodd, F. E.; Abraham, Z. H.; Eady, R. R.; Smith, B. E.; Hasnain, S. S. *J. Mol. Biol.* **1999**, *287*, 1001−1009.
(23) Armstrong, F. A.; Heering, H. A.; Hirst, J. *Chem. Soc. Rev.* **1997**, *26*, 169−179.
(24) Heering, H. A.; Hirst, J.; Armstrong, F. A. *J. Phys. Chem. B* **1998**, *102*, 6889−6902.
(25) Léger, C.; Elliott, S. J.; Hoke, K. R.; Jeuken, L. J. C.; Jones, A. K.; Armstrong, F. A. *Biochemistry* **2003**, *42*, 8653−8662.
(26) Wijma, H. J.; Macpherson, I.; Alexandre, M.; Diederix, R. E.; Canters, G. W.; Murphy, M. E.; Verbeet, M. P. *J. Mol. Biol.* **2006**, *358*, 1081−1093.
(27) Lide, D. R. *CRC Handbook of Chemistry and Physics*, 86th ed.; CRC Press: Boca Raton/London/New York/Singapore, 2005; pp 8−81.

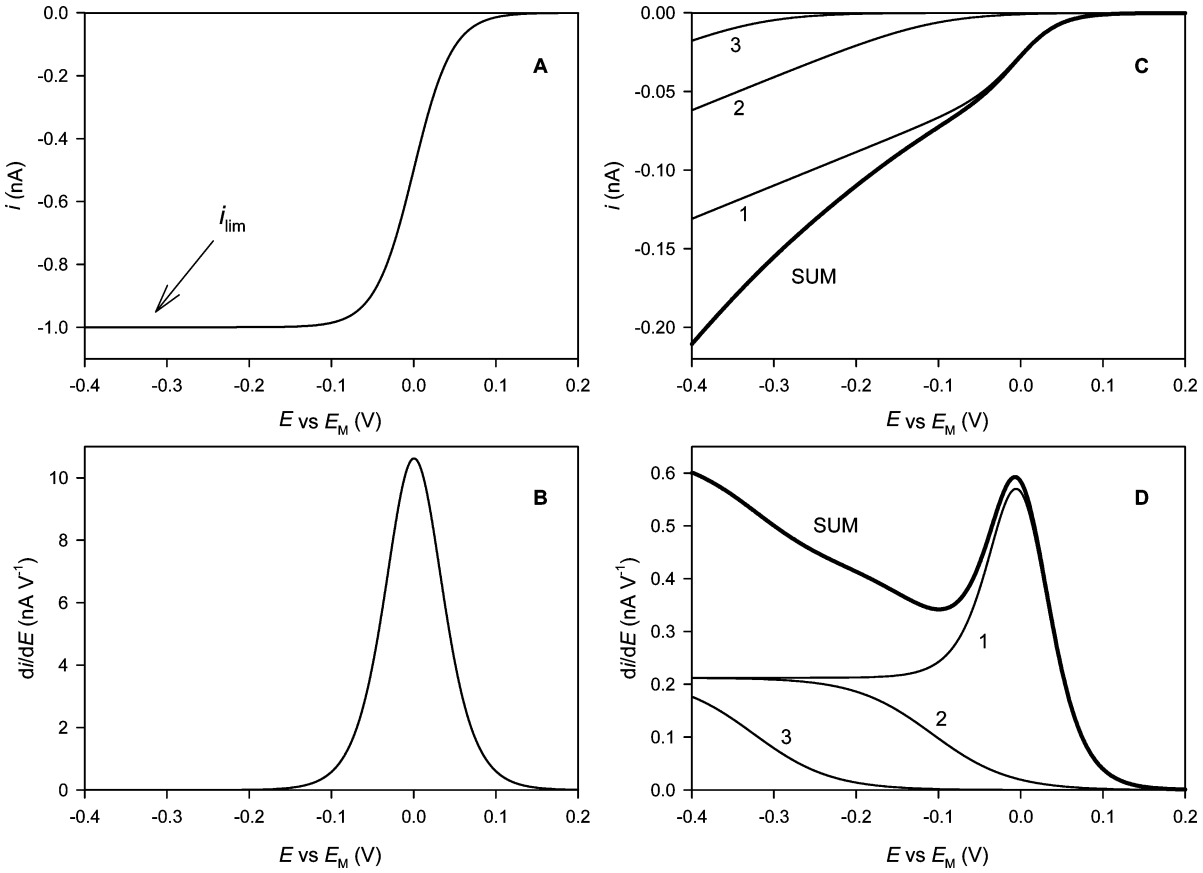

Figure 1. Effect of heterogeneity on catalytic voltammograms for a one-electron reductase with type-1 and type-2 Cu sites. Catalytic voltammograms calculated on the basis of eq 5. The value of i_{lim} is normalized to 1 nA reduction current and $E_M = 0$ mV for all plots. (A) Voltammogram (i versus E curve) when electron transfer with the electrode and electron transfer within the enzyme are fast. The catalytic current is determined by k_t and E_M of the type-2 site according to the Nernst equation. The resulting shape of the catalytic response is shown. (B) The first derivative of the curve shown in panel A. (C) Voltammograms calculated (see eq 5) by assuming that the distances between the redox site and the electrode are distributed over a range d_R; k_0^{max} is the rate of electron transfer when the type-1 center is closest to the electrode. For a trimeric enzyme, there are three sets of k_t/k_0^{max} (labeled A, B, and C), while d_R is assumed to be identical for each monomer. In the present example, the following values were chosen: $k_t/k_0^{max\_A} = 0.01$ (trace 1), $k_t/k_0^{max\_B} = 10$ (trace 2), $k_t/k_0^{max\_C} = 1000$ (trace 3), and $\beta d_R = 100$. (D) First derivatives of the traces shown in panel C. See text for further details.

enzyme in the IRS), k_t will increase with time (nitrite indirectly draws the enzyme out of the IRS by depleting the reduced water-bound type-2 site; direct binding of nitrite to the IRS can be ruled out on the basis of the nitrite concentration dependence of the inactivation rates, *vide infra*). Using Scheme 1, it can be shown[28] that the rates of activation (k_{act}) and inactivation (k_{inact}) are identical[29] and depend on nitrite concentration according to

$$k_{act} = k_{inact} = k_{-5} + k_5\left(\frac{1 + K_A[NO_2^-]}{1 + K_B[NO_2^-] + K_C[NO_2^-]^2}\right) \quad (3)$$

with

$$K_A \equiv \frac{k_1k_3k_{-4}}{k_2(k_6 + k_{-4})(k_{-1} + k_3)} \quad (3a)$$

$$K_B \equiv \frac{k_1k_3k_{-4} + k_4k_{-1}k_6 + k_4k_3k_6 + k_4k_2k_{-1} + k_4k_2k_3}{k_2(k_6 + k_{-4})(k_{-1} + k_3)} \quad (3b)$$

$$K_C \equiv \frac{k_1k_4(k_6 + k_3)}{k_2(k_{-1} + k_3)(k_6 + k_{-4})} \quad (3c)$$

(28) Huang, C. Y. *Methods Enzymol.* **1979**, *63*, 54−84.
(29) Fersht, A. *Enzyme Structure and Mechanism*; W. H. Freeman and Co.: New York, 1985; p 136.

Equation 3 contains more parameters than can be extracted reliably by fitting the data, but it does show that, when the nitrite concentration approaches zero, $k_{act} = k_{-5} + k_5$, while at very high nitrite concentration, $k_{act} = k_{-5}$.

Potential Dependence of Current. The dependence of enzymatic current (i) on electrode potential yields information on the midpoint potential of the active site and/or that of its electron relay centers. The simplest model[24,25] with which to analyze the dependence of the NiR enzymatic current on electrode potential is one in which electron transfer between electrode and type-2 active site (interfacial and intramolecular via the type-1 site) is fast compared to the turnover rate of the enzyme k_t. Within this limit, depletion of electrons from the type-2 site via turnover of nitrite is too slow to disturb the redox equilibrium between the electrode and both type-1 and type-2 sites. Then, because i is proportional to the fraction of reduced type-2 sites, the catalytic current depends on the electrode potential according to the Nernst equation (Figure 1A). The first derivative (Figure 1B) of this catalytic voltammogram shows a single symmetrical peak with a maximum at the position of the midpoint potential (E_M) of the electrochemical "control center" of the enzyme[25]—that is, the center along an ET pathway up to which electron exchange with the electrode is fast. (Note that the rate-determining step in catalytic electron flow will thus occur after the control center.) Because our simple model invokes fast electron transfer between the type-2 and type-1 Cu centers, this midpoint potential should correspond to the type-2 site, and the limiting current (i_{lim}) in Figure 1A corresponds to the activity of the enzyme when the type-2 site is 100% reduced. An alternative scenario is that electron transfer between

type-1 and type-2 centers is slow, in which case the potential E_M corresponds to the type-1 site and the turnover rate k_t depends on the fraction of reduced type-1. The current i_t is directly related[24] to the catalytic rate k_t via

$$i_t = k_t F A \Gamma \tag{4}$$

in which F is Faraday's constant, A is the surface area of the electrode, and Γ is the surface coverage expressed in active subunits of NiR per unit area.

Yet another scenario is that a fraction of the immobilized NiRs are oriented on the electrode in a nonoptimal manner and electron transfer between the electrode and the type-1 site (the electron entry point) is rate-limiting.[30] This situation can be modeled[30] with three extra parameters: a range of distances (d_R) between electrode and redox center, the decay constant β for electron transfer (βd_R in eq 5), and the rate of electron transfer when the enzyme is optimally oriented for electron transfer to the electrode (k_0^{max}). With an even distribution of enzyme molecules having a tunneling distance in the range d_R, the model predicts[30] a linear increase in current with increasing driving force (Figure 1C). This nonideality is, indeed, found for most immobilized enzymes but need not be too detrimental.[30] In the derivative of the catalytic voltammogram (Figure 1D), a peak still occurs at the midpoint potential of the control center unless k_t/k_0^{max} is so low that that the peak becomes negligible compared to the subsequent linear increase in current versus electrode potential.

Equation 5 describes the dependence of catalytic current on electrode potential (E) for a one-electron reductase displaying heterogeneity with respect to orientation on the electrode. Equation 5 was derived along the same lines as used[30] for a two-electron reductase:

$$i = \frac{i_{lim}}{\beta d_R} u \frac{1}{1+\upsilon^2} \tag{5}$$

with

$$u \equiv \ln\left(\left(1+\upsilon^2+\frac{k_t}{k_0^{max}}\upsilon\right)/\frac{k_t}{k_0^{max}}\upsilon\right) \tag{5a}$$

$$\upsilon \equiv \exp\left[\frac{F}{2RT}(E-E_M)\right] \tag{5b}$$

The fitted parameters in eq 5 are E_M, $i_{lim}/\beta d_R$, and k_t/k_0^{max}. Information about $i_{lim}/\beta d_R$ is contained in the slope of the i vs E plot, while the initial curvature reports on k_t/k_0^{max} and E_M. In the case of NiR, there is the added complication that there are three catalytic centers per molecule, that each may contribute to the catalytic current. The voltammograms were modeled, therefore, by using a population consisting of three subpopulations of active sites (close to the electrode, farther away, and farthest away, see Figure 1C,D). The data were fitted to single values of E_M and $i_{lim}/\beta d_R$, and three values of k_t/k_0^{max}, i.e., $k_t/k_0^{max\_A}$, $k_t/k_0^{max\_B}$, $k_t/k_0^{max\_C}$, corresponding to the three subunits according to eq 6,

$$\frac{di}{dE} = -\frac{i_{lim}}{\beta d_R}\frac{F}{2RT}\frac{1+2u(\upsilon^2+\upsilon^4+(k_t/k_0^{max})\upsilon^3)-\upsilon^4}{(1+\upsilon^2+(k_t/k_0^{max})\upsilon)(1+\upsilon^2)^2} \tag{6}$$

which is the first derivative of eq 5. The E_M value is far more conspicuous in the first derivative compared to the normal voltammogram (compare the sum traces in panels C and D of Figure 1). In eqs 5 and 6, R is the gas constant, and T is the absolute temperature.

Results and Discussion

Reductive Inactivation. Nitrite reductase (NiR) immobilized on a PGE electrode is catalytically active. In the presence of nitrite, a strong catalytic current is observed as the electrode potential is taken below 0.3 V versus NHE (Figure 2A). This current continues to increase as the potential is taken more negative, indicating that a substantial population of the enzyme molecules undergo slow electron transfer from the electrode (see Material and Methods). In the absence of nitrite, no voltammetric features were present that could be assigned to the type-1 or type-2 sites, which suggests that the surface coverage of the enzyme is too low (below 3 pmol cm^{-2} [31]) for a signal to be detectable.[32]

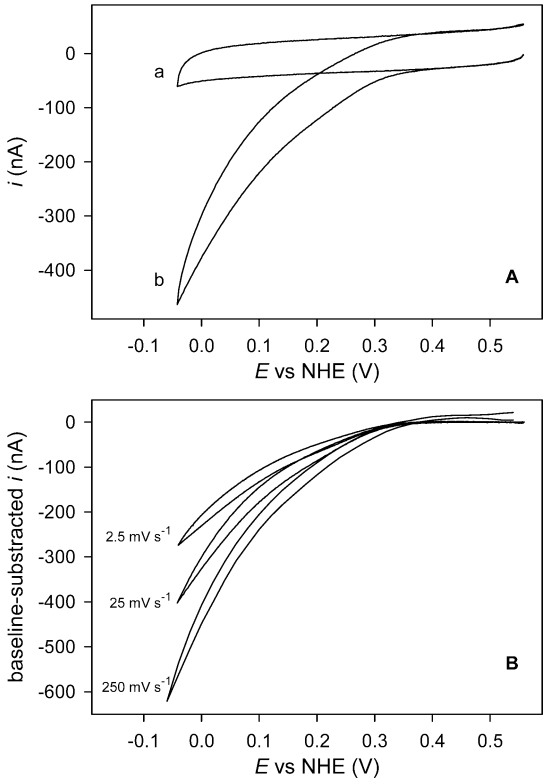

Figure 2. Effect of scan rate on catalytic amplitude. (A) Cyclic voltammogram in the absence (a) and in the presence (b) of nitrite (1 mM), scan rate 25 mV s^{-1}. (B) Baseline-subtracted current (b − a) at different scan rates. The PGE electrode with the NiR film was rotated at 3000 rpm in malate/MES/HEPES buffer (each component 25 mM, 1 °C, pH 6.7).

By subtracting the capacitance, it was determined that, when commencing the sweep from the high-potential limit, the catalytic current observed on the forward scan (in the direction of negative potential) was always higher than that observed on the return scan (Figure 2B). When commencing the sweep from the low-potential limit, the reverse result was obtained (results not shown). Again, starting from the high-potential limit, variations in the scan rate reproducibly gave diminished catalytic currents at lower scan rates (Figure 2B). These observations suggest that a slow reductive inactivation occurs; i.e., at decreased scan rates, the inactive form has more time to accumulate at reducing potential. To investigate this further, controlled potential amperometric measurements were made.

The reductive inactivation was measured by first holding the electrode at an oxidizing potential (560 mV versus NHE, 100 s) to ensure that all enzyme was in the active state. After

(30) Léger, C.; Jones, A. K.; Albracht, S. P. J.; Armstrong, F. A. *J. Phys. Chem. B* **2002**, *106*, 13058−13063.

(31) Jones, A. K.; Lamle, S. E.; Pershad, H. R.; Vincent, K. A.; Albracht, S. P. J.; Armstrong, F. A. *J. Am. Chem. Soc.* **2003**, *125*, 8505−8514.

(32) From eq 4, assuming $k_t = 10^3$ s^{-1}, as measured in solution,[4] and $i_t = 500$ nA (Figure 2A), a surface coverage of ~0.1 pmol cm^{-2} was estimated.

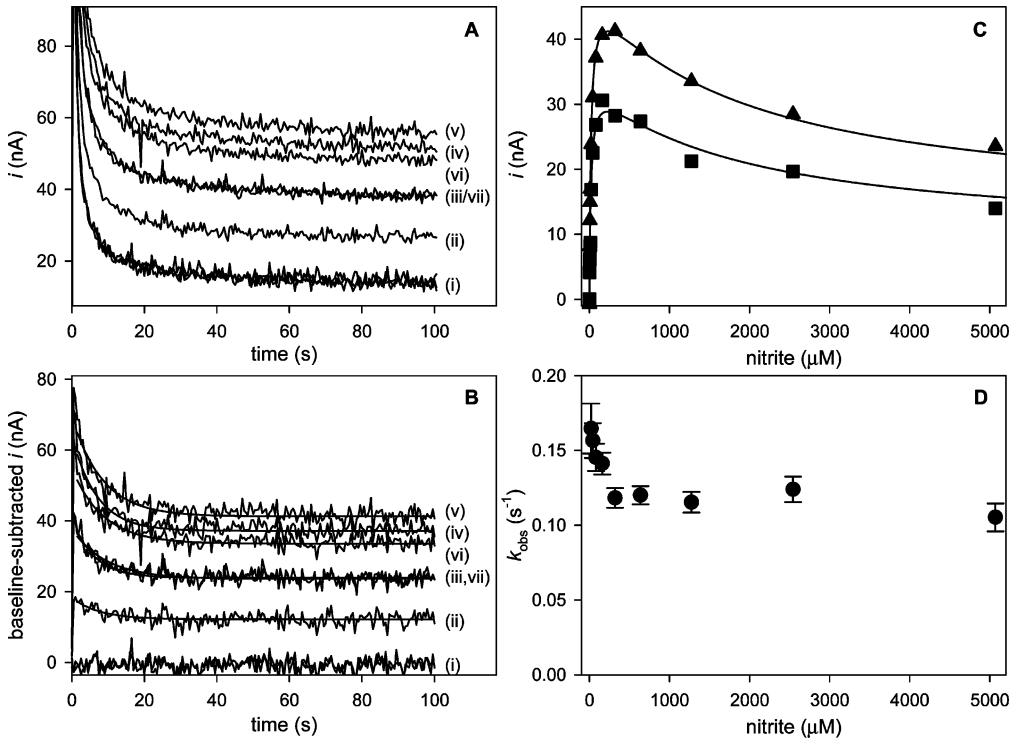

Figure 3. Chronoamperometry of PGE-immobilized nitrite reductase. (A) The electrode was poised at 560 mV versus NHE for 100 s, and the current was measured as a function of time after the potential was switched to 60 mV versus NHE. Traces measured for different concentrations of nitrite: (i) 0 μM (three traces); (ii) 5 μM; (iii) 20 μM; (iv) 80 μM; (v) 318 μM; (vi) 1.27 mM; (vii) 5.07 mM. (B) The traces shown in Figure 3A after subtraction of the average of the three traces (i). The resulting traces (ii)−(vii) were fitted (solid line) to a single exponential $[i(t) = i(\infty) + [i(0) - i(\infty)] \exp(-k_{obs}t)]$. Data for the first second after the start of the assay were not used for the fit. (C) Plot of the parameters obtained from the fits in panel B as a function of nitrite concentration. Triangles, $i(\infty)$; squares, $i(0) - i(\infty)$; lines, group fit to eq 2. Additional points represent data obtained at the following nitrite concentrations: 2.5 μM, 10 μM, 40 μM, 160 μM, 637 μM, and 2.54 mM. (D) Plot of k_{obs} versus nitrite concentration. Data obtained for experiments with less than 20 μM nitrite were omitted, as the errors were excessively large. For all panels the conditions were as stated in Figure 2, except that the pH was 5.3.

initiation of the catalytic turnover by stepping the potential to 60 mV versus NHE, the catalytic current was monitored over a short period of time (Figure 3A). The resulting decrease in catalytic activity was complicated by slow electrode charging effects, which could be measured independently in the absence of nitrite (traces labeled (i) in Figure 3A).[33] This contribution from the electrode surface was reproducible, and corrected time curves were produced by subtraction of the average of traces (i) from the traces (ii)−(vii), measured in the presence of nitrite. The resulting traces (Figure 3B) could be fitted with single exponentials with rate constants k_{obs}. The magnitude of the decrease ($i(0) - i(\infty)$) and the steady-state current ($i(\infty)$) were fitted as functions of $[NO_2^-]$ (Figure 3C) using eq 2. This procedure resulted in similar values of K_M^A, K_M^B, and k_{cat}^B/k_{cat}^A (Table 1), thus providing further evidence that both $i(\infty)$ and ($i(0) - i(\infty)$) reflect the true activity of NiR. On the basis of Scheme 1, it is expected that eq 2 should also apply when no IRS has yet formed.[21]

The observed *inactivation* rate constants, k_{obs}, are plotted as a function of $[NO_2^-]$ in Figure 3D. The $[NO_2^-]$ dependence is described by eq 3. Figure 3D shows that lower rates are observed at higher nitrite concentrations. This agrees with the predictions based on Scheme 1, in which a reduced *inactive* state equilibrates with an *active* state that is able to bind nitrite. The alternative, by which nitrite binds directly to the IRS, is ruled out as this would result in an increase in k_{obs} at higher nitrite concentrations, contrary to observations (Figure 3D). As remarked earlier, as the nitrite concentration approaches zero, $k_{obs} = k_5 + k_{-5}$, whereas at high nitrite concentrations, $k_{obs} = k_{-5}$. Thus, at pH 5.3, $k_5 + k_{-5} \approx 0.2\ s^{-1}$ and $k_{-5} \approx 0.1\ s^{-1}$ (Figure 3D).

Table 1. Kinetic Constants Obtained from Data Fitting

	K_M^A (μM)	K_M^B (μM)	k_{cat}^B/k_{cat}^A
Figure 3C:			
group fit to eq 2[a]	20 ± 2	(1.8 ± 0.5) × 10^3	0.3 ± 0.1
$i(\infty)$	16 ± 1	(2.4 ± 0.8) × 10^3	0.3 ± 0.1
$i(0) - i(\infty)$	27 ± 3	(1.1 ± 0.3) × 10^3	0.3 ± 0.1
Effect of glycerol:			
without glycerol[b]	40 ± 3	(2.4 ± 0.6) × 10^3	0.3 ± 0.1
with glycerol[c]	61 ± 2	(3.6 ± 0.5) × 10^3	0.32 ± 0.03

[a] Data points of both $i(\infty)$ and $i(0) - i(\infty)$ were fitted simultaneously to eq 2 to obtain the values for k_{cat}^B/k_{cat}^A, K_M^A, and K_M^B. [b] pH 5.95. [c] pH 6.05.

We also investigated the *activation of prereduced* NiR by the addition of nitrite. First the steady-state current was measured as a function of nitrite concentration (Figure 4A).[34] The activity shows a maximum around 300 μM (see arrow 1 in Figure 4A). In the next experiment, the electrode was first poised at a reducing potential (60 mV versus NHE), after which a 320 μM concentration of nitrite was added to the solution (see Figure 4B, arrow 1). The current showed a rapid increase followed by a slower, exponential phase, with $k_{obs} = 0.2\ s^{-1}$, which we ascribe to slow activation of the inactive form of the enzyme.

(33) Armstrong, F. A.; Camba, R.; Heering, H. A.; Hirst, J.; Jeuken, L. J.; Jones, A. K.; Leger, C.; McEvoy, J. P. *Faraday Discuss.* **2000**, 191−203.

(34) This figure is similar to Figure 3C but with a logarithmic abscissa. The higher current achieved in this experiment is due to a higher surface coverage of the enzyme.

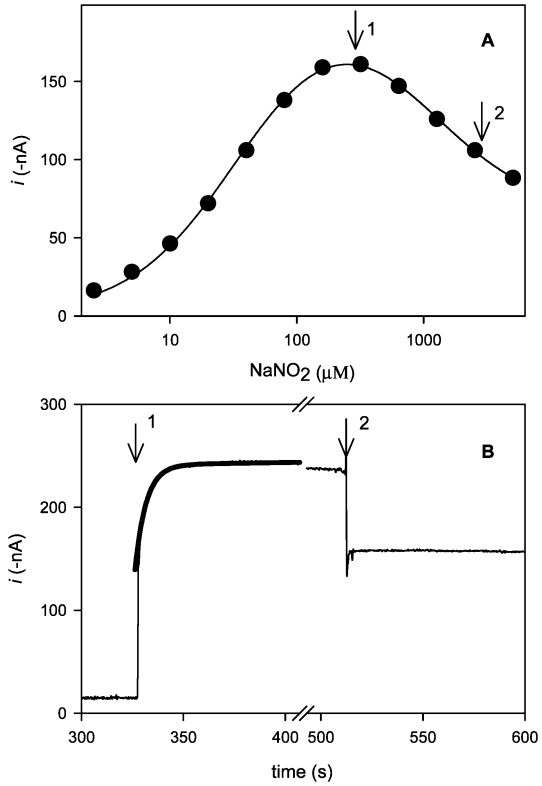

Figure 4. Reactivation of NiR on a rotating disk electrode. Chronoamperometry of PGE-immobilized NiR. (A) Semi-logarithmic plot[34] of steady-state current versus nitrite concentration (pH 5.5). The solid line is a fit to eq 2 (the catalytic current is proportional to k_t in eq 2), yielding $V^A = -2.1 \times 10^{-8}$ A, $K_M{}^A = 36$ μM, $K_M{}^B = 1.0$ mM, and $k_{cat}{}^B/k_{cat}{}^A = 0.3$. (B) Catalytic current as a function of time. At $t = 325$ s, nitrite was injected to give a concentration of 320 μM (arrow 1). At $t = 510$ s, a second addition of nitrite was made (arrow 2, to a final concentration of 3200 μM). The small initial current is the background (corrected for in panel A). The exponential fit is indicated with a thick line (panel B). The experiments in panels A and B were carried out on different enzyme films (resulting in slightly different amplitudes). The electrode was rotated at 4000 rpm.

Table 2. Rates of Inactivation and Activation versus Electrode Potential[a]

E vs NHE (V)	k_{act} (s^{-1})	k_{inact} (s^{-1})
−0.19	0.20 ± 0.03	0.29 ± 0.06
−0.07	0.17 ± 0.05	0.26 ± 0.07
0.11	0.17 ± 0.02	0.20 ± 0.03

[a] The rate of *activation* was measured by changing the nitrite concentration in a single step from 0 to 320 μM (Figure 4B, arrow 1), while the rate of *inactivation* was measured as illustrated in Figure 3A after a stepwise increase of electrode potential at 3200 μM nitrite (both at pH 5.6).

To check to what extent the mixing time of the added nitrite might affect the time behavior of the current, a second addition of nitrite was made to give a solution concentration of 3200 μM nitrite (Figure 4A, arrow 2). From Figure 4B, it is clear that this higher concentration (arrow 2) causes immediate inhibition and that the time needed for the added nitrite to mix with the solution plays no detectable role.

The data in Figure 4B (arrow 1) indicate approximately equal amounts of reduced NiR with active and inactive type-2 sites in the absence of nitrite; thus, we find again that k_5 is approximately equal to k_{-5}. The rates of inactivation and activation have been collected in Table 2. It is clear that the rates do not depend on the electrode potential in the range −200 to +100 mV versus NHE (Table 2).

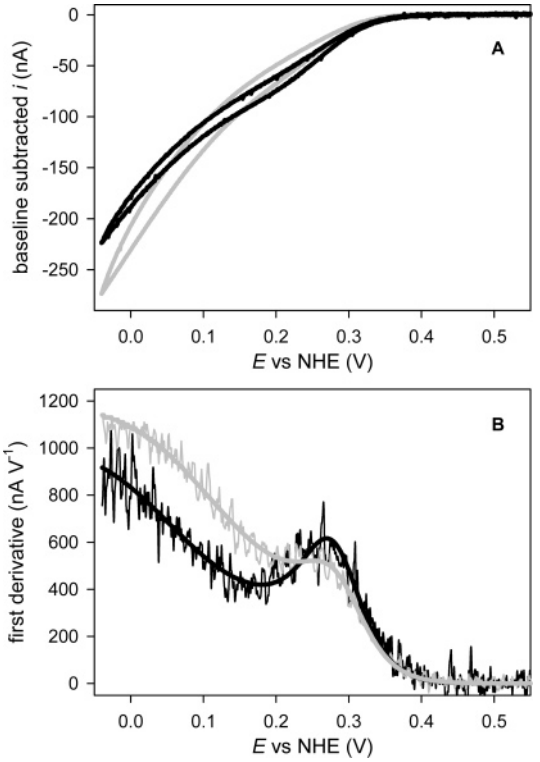

Figure 5. Effect of glycerol on shape of voltammogram. (A) Cyclic voltammograms scanned at 2.5 mV s^{-1} at pH 6.7, with 1 mM nitrite in the absence of glycerol (gray line) and in the presence of 20% glycerol (black line). (B) First derivatives and fits (solid lines) of these scans (same color code). The fit to eq 6 produced the following values (the values in the presence of glycerol are in parentheses): $E_M = 286$ mV versus NHE (281 mV), $k_t/k_0{}^{max\_A} = 0.22$ (0.06), $k_t/k_0{}^{max\_B} = 18$ (58), $k_t/k_o{}^{max\_C} = 105$ (279), $i_{lim}/\beta d_R = -18.5$ nA (−15.9 nA).

Dependence of Catalytic Activity on Electrode Potential and Nitrite Concentration. The catalytic voltammograms were investigated further in the absence and in the presence of glycerol (Figure 5) and as a function of nitrite concentration (Figure 6) to obtain more information about the nature of the ET processes occurring between electrode and immobilized NiR. The scan rates used (1−2.5 mV s^{-1}) were slow enough to ensure equilibrium between active and inactive forms of the reduced NiR (as shown by the semi-reversible traces in Figures 5A and 6). Slow, irreversible loss of enzyme activity precluded the use of even slower scan rates. (The loss of activity amounts to a few percent on a time scale of 100 s; see, for instance, the small change in activity in Figure 4B in the 400−500 s interval.) Again, rather than reaching a constant plateau, the catalytic current increased steadily at potentials more negative than E_M (Figure 5), suggesting a spread of electron tunneling distances between the electrode and the electron entry point of the enzyme. As explained in the Materials and Methods section, the derivative curve (Figure 5B, gray line) was fitted by three subpopulations reflecting the trimeric structure of NiR (see caption of Figure 5 for values). In the presence of 20% glycerol, the peak marking the E_M value is more conspicuous (Figure 5B). From the fitted values of $k_t/k_0{}^{max}$ for the different subpopulations, it appears that glycerol improves the electronic coupling to the closest subpopulation of type-1 sites (see Figure caption). The midpoint potential was approximately the same in the presence (281 mV versus NHE) and in the absence (286 mV versus NHE) of glycerol, as were the values for $K_M{}^A$, $K_M{}^B$,

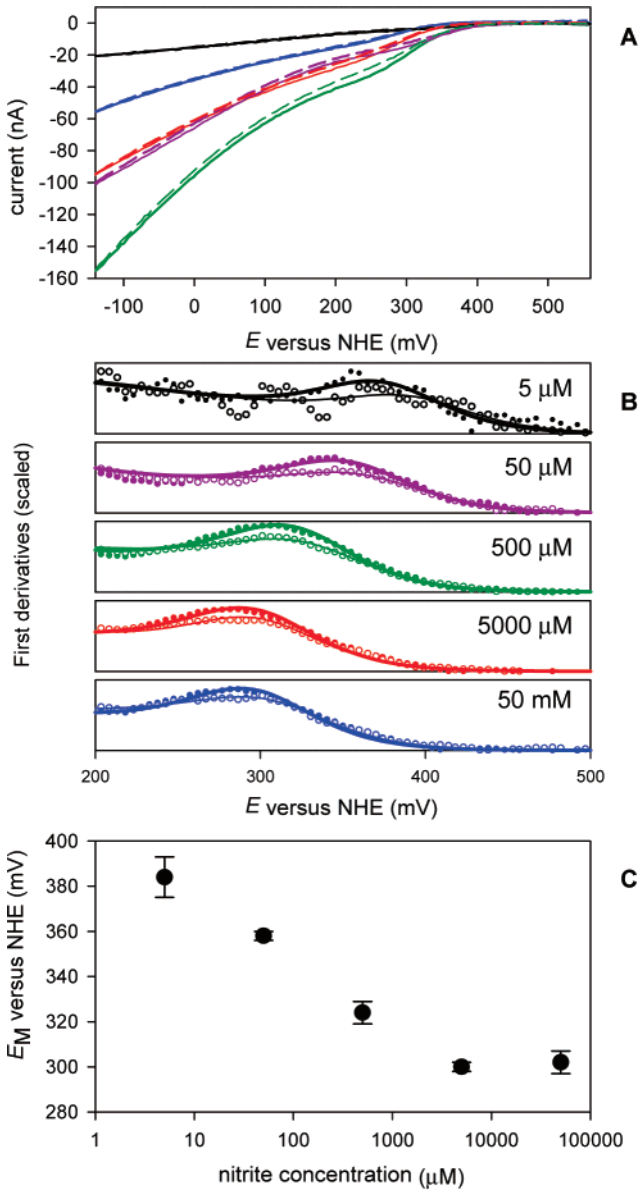

Figure 6. Observed midpoint potential versus nitrite concentration. (A) Baseline-corrected voltammograms at a scan rate of 1 mV s^{-1} at pH 5.6 for nitrite concentrations increasing from 5 μM to 50 mM (see lower panels for color code). Continuous lines denote forward scans, from positive to negative potential, and dashed lines denote backward scans. (B) First derivatives fitted with eq 6. Closed circles are the data from the forward scans and are fitted with a thick line, while open circles are the data for the backward scans that are fitted with a thin line. (C) E_M values as a function of nitrite concentration.

and $k_{cat}{}^{B}/k_{cat}{}^{A}$ (Table 1). Thus, addition of glycerol resulted in a more precise determination of E_M, although it did not alter the catalytic properties of the enzyme.

The dependence of E_M on nitrite concentration was studied in some detail, and the voltammograms and their derivatives are reproduced in Figure 6A,B, respectively. A gradual decrease from 385 to 300 mV was observed upon increasing the nitrite concentration from 5 μM to 5 mM (Figure 6C), while E_M remained constant beyond 5 mM (up to 50 mM). The simplest explanation for this observation is that, at increasing nitrite concentrations, route B in Scheme 1 prevails[21] and that, with nitrite bound to the type-2 site, the type-1 → type-2 electron transfer (step 3) is much slower than electron exchange between the type-1 site and the electrode. Therefore, as $[NO_2^-]$ is increased, E_M gradually approaches the midpoint potential of the type-1 site. For the related NiR from *Achromobacter cycloclastes* (82% identical amino acid sequence), it was indeed found that the type-2 site midpoint potential is 50 mV higher than the type-1 site potential at pH 6.[35]

Catalytic voltammograms at saturating nitrite concentrations (Figure 7A) were recorded over the pH range 5−8.5. The pH dependence of the midpoint potential of the type-1 site was also determined by potentiometric titrations under the same conditions.[36] Oxidative and reductive titrations gave identical results (Figure 7B). As the pH is raised, the E_M value (Figure 7C) decreases by 100 mV. Over the range pH 4.8−8.8, the midpoint potentials of the type-1 site, as determined by the potentiometric titrations (Figure 7C, circles with error bars), were identical to the E_M values determined in catalytic voltammograms at saturating nitrite concentration (squares). This shows that, at saturating nitrite concentration, the reduction of the type-2 site is rate-limiting and that the midpoint potential of the type-1 site is not altered by nitrite binding to the type-2 site.

A catalytic current could be observed with nitric oxide as the substrate, but this was restricted to a narrow pH range (Figure 8A). In experiments conducted at 1 °C, the catalytic oxidation of nitric oxide is barely detectable at pH 7 (a few nanoamperes at 0.6 V versus NHE), increases to a maximum that is stable from pH 8 to 9, and then decreases and is no longer detectable at pH 10 (baseline subtraction became too cumbersome at the latter pH, and the trace is not shown in Figure 8A). Increasing the scan rate from 5 to 25 mV s^{-1} did not influence the current amplitudes, and reversible inactivation could not be detected under these conditions. We compared the catalytic current, on a single protein film, for either nitrite or nitric oxide (Figure 8B). The slopes of the catalytic current are equal to $i_{lim}F/\beta d_R 2RT$ (eq 6); therefore, the ratio of the slopes equals the catalytic bias of the enzyme on the electrode ($i_{lim}{}^{forward}/i_{lim}{}^{reverse} \approx 2$ at pH 6.8, 20 °C, Figure 8B), which is in reasonable agreement with the known catalytic bias ($k_{cat}{}^{forward}/k_{cat}{}^{reverse} = 6$, pH 7.0, 25 °C[4]) in solution.

Summary and Conclusions

The similarity in catalytic bias (Figure 8) and steady-state kinetics between solution studies[21] and the present PFV results indicate that NiR immobilized on a graphite electrode has the same catalytic properties as in solution. Earlier, using scanning probe microscopy, it was observed that nitrite reductases from other organisms remain intact when immobilized on a gold electrode.[37,38] The shapes of the catalytic voltammograms can be fitted assuming that the trimeric structure of NiR results in slower ET rates between the electrode and the type-1 centers that are farther away from the electrode. The close agreement between E_M obtained from the catalytic voltammograms and E_M obtained from potentiometric titrations (Figure 7C) shows that the modeling is sufficiently accurate for conclusions to be drawn.

Both cyclic voltammograms (Figure 2) and chronoamperometry (Figures 3 and 4, Table 1) are consistent with Scheme

(35) Kobayashi, K.; Tagawa, S.; Deligeer Suzuki, S. *J. Biochem.* (*Tokyo*) **1999**, *126*, 408−412.
(36) pH 4−9, 20% glycerol, mixed malate/MES/HEPES buffer, 1 °C.
(37) Zhang, J.; Welinder, A. C.; Hansen, A. G.; Christensen, H. E. M.; Ulstrup, J. *J. Phys. Chem. B* **2003**, *107*, 12480−12484.
(38) Contera, S.; Iwasaki, H. *Ultramicroscopy* **2002**, *91*, 231−243.

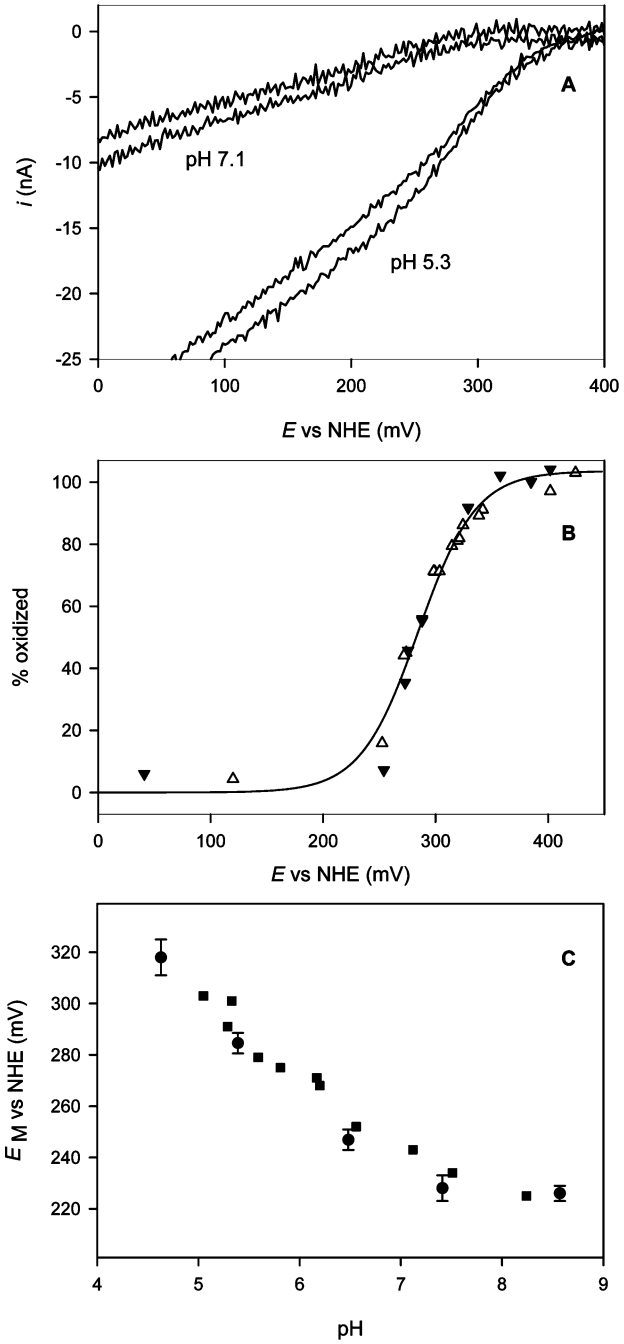

Figure 7. pH dependence of the midpoint potential of the type-1 center. (A) Example of background-subtracted voltammograms (1 mV s^{-1}) at two different pH values (5.3 and 7.1). (B) Example of a potentiometric titration (at pH 5.4). The open triangles are of the oxidizing titration, and the closed triangles are of the reductive titration. The solid line is a fit of all data to the Nernst equation. (C) Plot of the midpoint potentials E_M versus pH. Squares depict E_M values as obtained from the PFV measurements at saturating nitrite concentrations (10 mM between pH 5 and 5.6, 50 mM between pH 5.8 and 6.2, 100 mM above pH 6.2). Circles with error bars depict E_M values of the type-1 site obtained from potentiometric titrations.

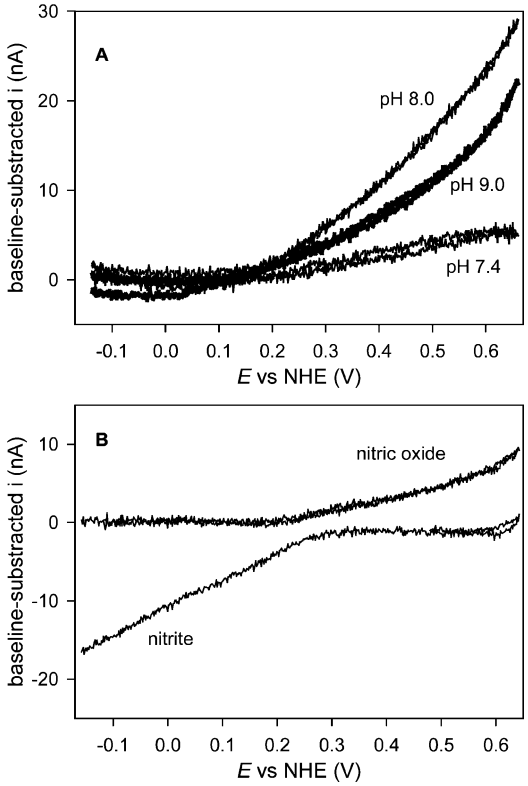

Figure 8. Nitric oxide oxidation by PGE-immobilized NiR. Baseline-corrected voltammograms of PGE-immobilized NiR in the presence of NO. The scans were started at a reducing potential. (A) Cyclic voltammograms at 1 °C obtained in the presence of 16 μM nitric oxide at a scan rate of 5 mV s^{-1}. Scans at different pH values are from different protein films. (B) Voltammograms recorded in the presence of either nitrite or nitric oxide with a single protein film, 20 °C, pH 6.8, and a scan rate of 1 mV s^{-1}. The buffer consisted of 25 mM concentrations of each of the buffer components (malate, MES, HEPES, TAPS, CHES, and CAPS) and was adjusted to the desired pH using NaOH. The nitrite concentration was 10 mM; the nitric oxide concentration was 16 μM.

1. The novelty of Scheme 1 is that there is an equilibrium between two conformations of the reduced type-2 site: an active one, in which the type-2 site binds nitrite, and the IRS, in which the type-2 site does not bind nitrite. Earlier it was concluded[22] from EXAFS and X-ray crystallography[17−20] that that the reduced type-2 site was three- instead of four-coordinate and incapable of binding nitrite or other external ligands. The IRS that we observe possibly corresponds to this three-coordinated species.[17−20,22] Figures 2 and 3 show that, during catalytic turnover, a significant part of the NiR is inactivated. Most importantly, our data show that the inactivation of active reduced state to IRS is slow and reactivation of the reduced NiR is possible. This has profound implications for understanding the catalytic cycle of NiR and the properties of the reduced type-2 site.

The presence of the IRS as a function of pH has not been investigated in this study. In preliminary experiments at alkaline pH, similar to the experiments presented in Figure 3, an exponential decrease in current is less pronounced or absent. This is a subject of further investigation. The occurrence of a three-coordinated Cu species is not unprecedented.[39−42] Type-1 Cu sites have a tendency to change their coordination from four to three upon reduction, and the same may apply to type-2 sites like the IRS in our case. It is conceivable that binding of a neutral fourth ligand, like a water molecule, by the three-coordinate reduced copper is thermodynamically still a pos-

(39) Gray, H. B.; Malmstrom, B. G.; Williams, R. J. *J. Biol. Inorg. Chem.* **2000**, *5*, 551−559.
(40) Guss, J. M.; Harrowell, P. R.; Murata, M.; Norris, V. A.; Freeman, H. C. *J. Mol. Biol.* **1986**, *192*, 361−387.
(41) Canters, G. W.; Kolczak, U.; Armstrong, F.; Jeuken, L. J.; Camba, R.; Sola, M. *Faraday Discuss.* **2000**, 205−220; discussion 257−268.
(42) Jeuken, L. J. C.; van Vliet, P.; Verbeet, M. P.; Camba, R.; McEvoy, J. P.; Armstrong, F. K.; Canters, G. W. *J. Am. Chem. Soc.* **2000**, *122*, 12186−12194.

sibility at room temperature, while the binding of a charged ligand, like nitrite or a hydroxide ion, is not.

The catalytic voltammograms obtained at saturating nitrite concentration (Figures 6 and 7) are in agreement with a rate-limiting type-1 → type-2 ET step. This was inferred earlier on the basis of less direct evidence (activation energy and steady-state kinetics).[21,43] The midpoint potential of the type-1 site is not altered by nitrite binding to the type-2 site (Figure 7B), which rules out any cooperativity between the type-1 and type-2 sites during the catalytic cycle.

Acknowledgment. H.J.W. acknowledges Dr. H. A. Heering for useful discussions and Dr. K. A. Vincent for help with some electrochemical experiments. L.J.C.J. acknowledges useful discussions with Dr. C. Léger regarding the derivation of eq 5. Research in the F.A.A. group was supported by the BBSRC (43/B19096). L.J.C.J. was supported by a BBSRC David Phillips fellowship (24/JF/19090).

JA071274Q

(43) Zhao, Y.; Lukoyanov, D. A.; Toropov, Y. V.; Wu, K.; Shapleigh, J. P.; Scholes, C. P. *Biochemistry* **2002**, *41*, 7464−7474.